EJNMMI Research
a SpringerOpen Journal

ORIGINAL RESEARCH Open Access

Evaluation of efficacy of a new MEK inhibitor, RO4987655, in human tumor xenografts by [^{18}F] FDG-PET imaging combined with proteomic approaches

Tetyana Tegnebratt[1*], Elisabeth Ruge[2], Sabine Bader[3], Nobuya Ishii[4], Satoshi Aida[4], Yasushi Yoshimura[4], Chia-Huey Ooi[3], Li Lu[1], Nicholas Mitsios[6], Valerie Meresse[5], Jan Mulder[6], Michael Pawlak[7], Miro Venturi[2], Jean Tessier[5] and Sharon Stone-Elander[1]

Abstract

Background: Inhibition of mitogen-activated protein kinase (MEK, also known as MAPK2, MAPKK), a key molecule of the Ras/MAPK (mitogen-activated protein kinase) pathway, has shown promising effects on *B-raf*-mutated and some RAS (rat sarcoma)-activated tumors in clinical trials. The objective of this study is to examine the efficacy of a novel allosteric MEK inhibitor RO4987655 in *K-ras*-mutated human tumor xenograft models using [^{18}F] FDG-PET imaging and proteomics technology.

Methods: [^{18}F] FDG uptake was studied in human lung carcinoma xenografts from day 0 to day 9 of RO4987655 therapy using microPET Focus 120 (CTI Concorde Microsystems, Knoxville, TN, USA). The expression levels of GLUT1 and hexokinase 1 were examined using semi-quantitative fluorescent immunohistochemistry (fIHC). The *in vivo* effects of RO4987655 on MAPK/PI3K pathway components were assessed by reverse phase protein arrays (RPPA).

Results: We have observed modest metabolic decreases in tumor [^{18}F] FDG uptake after MEK inhibition by RO4987655 as early as 2 h post-treatment. The greatest [^{18}F] FDG decreases were found on day 1, followed by a rebound in [^{18}F] FDG uptake on day 3 in parallel with decreasing tumor volumes. Molecular analysis of the tumors by fIHC did not reveal statistically significant correlations of GLUT1 and hexokinase 1 expressions with the [^{18}F] FDG changes. RPPA signaling response profiling revealed not only down-regulation of pERK1/2, pMKK4, and pmTOR on day 1 after RO4987655 treatment but also significant up-regulation of pMEK1/2, pMEK2, pC-RAF, and pAKT on day 3. The up-regulation of these markers is interpreted to be indicative of a reactivation of the MAPK and activation of the compensatory PI3K pathway, which can also explain the rebound in [^{18}F] FDG uptake following MEK inhibition with RO4987655 in the *K-ras*-mutated human tumor xenografts.

Conclusions: We have performed the first preclinical evaluation of a new MEK inhibitor, RO4987655, using a combination of [^{18}F] FDG-PET imaging and molecular proteomics. These results provide support for using preclinical [^{18}F] FDG-PET imaging in early, non-invasive monitoring of the effects of MEK and perhaps other Ras/MAPK signaling pathway inhibitors, which should facilitate a wider implementation of clinical [^{18}F] FDG-PET to optimize their clinical use.

Keywords: ^{18}F FDG-PET; RO4987655; MAPK/PI3K pathway; RPPA; Signaling; Feedback loops

* Correspondence: tetyana.tegnebratt@ki.se
[1]Karolinska Institutet and Department of Neuroradiology, R3:00, MicroPET and Clinical Neurosciences, Karolinska University Hospital, Stockholm 17176, Sweden
Full list of author information is available at the end of the article

Background

The inhibition of integral components of the Ras/Raf/mitogen-activated protein kinase kinase (MEK)/extracellular signal-regulated kinase (ERK) signaling pathway has been proven clinically effective in *B-raf* melanoma and suggested to be effective in some RAS-activated tumors [1,2]. MEK has a critical position in this pathway with some direct upstream activators (e.g. Raf) and some downstream targets (e.g. ERK) and has been identified as a promising target for selective inhibition of *K-ras* and *B-raf*-mutated tumor types [3,4]. Many MEK inhibitors have been developed and have entered preclinical efficacy testing. Consequently, the need for new translational pharmacodynamic (PD) biomarkers for MEK inhibition efficacy in cancer treatment is increasing.

Non-invasive positron emission tomography (PET) imaging with the fluorine-18 labeled glucose analog 2-fluoro-2-deoxy-D-glucose ([^{18}F] FDG) is being used as a functional endpoint in phase I to III clinical trials in oncology for assessing therapeutic response, in addition to conventional endpoints such as toxicity in tumor size. Fluorine-18-labeled glucose analog 2-fluoro-2-deoxy-D-glucose-positron emission tomography ([^{18}F] FDG-PET) imaging has been used for monitoring neoadjuvant chemotherapy in patients with locally advanced breast cancer [5], non-small cell lung cancer [6], and lymphomas [7], for an early prediction of response to imatinib mesylate (Glivec^{TM}) in patients with advanced soft tissue sarcoma [8] and in the evaluation of vemurafenib (Zelboraf^{TM}), an oral *B-raf* inhibitor [9]. Several recent phase I dose-escalation clinical trials have also included [^{18}F] FDG-PET, for instance in assessing MEK inhibition as a monotherapy or in combination with other drugs in patients with advanced solid tumors [10-12].

PET imaging of small animals is increasingly used as a translational efficacy biomarker in anti-cancer drug development. Despite the inclusion of [^{18}F] FDG-PET as a possible clinical efficacy biomarker for MEK inhibition, very few preclinical studies have yet been performed to evaluate the nature and extent of its pharmacodynamic and/or predictive capability. In addition, it is critical for interpreting clinical data that the biological mechanisms related to changes in [^{18}F] FDG uptake are fully elucidated, a task for which pre-clinical experimentations is particularly well-suited. [^{18}F] FDG-PET/CT and MRI were used to show the synergistic effects of NVP-BEZ235, a dual PI3K/mTOR inhibitor, with the MEK inhibitor selumetinib in *K-ras*-mutated lung adenocarcinoma xenografts [10,13] and of the combination of PI3K/mTOR inhibitor PE-04691502 and MEK inhibitor PD0325901 in a mouse model of ovarian cancer [14]. Metabolic [^{18}F] FDG-PET responses could also monitor combination therapy with docetaxel and the MEK inhibitor selumetinib in mice with lung cancer [15]. Recently, [^{18}F] FDG-PET was used as an early PD biomarker of the efficacy of MEK inhibitor RO5126766 in human colorectal cancer xenografts with *K-ras* and *B-raf* mutations [16]. It was shown to be a sensitive biomarker not only for predicting efficacy but also acquired resistance in *B-raf*^{V600} mutant melanoma xenografts in mice treated with vemurafenib alone and in combination with the MEK inhibitor GDC-0973 [17].

Reverse phase protein array (RPPA) analysis is a high throughput antibody-based technology for large-scale analyses and quantitative assessments of activated signaling pathways and identification of biomarkers [18,19]. Multiplex analyses of PD biomarkers by RPPA have been performed *in vitro* in cancer cell lines [20,21] as well as in cancer tissue and blood samples [22-24] in order to assess response to target inhibition.

The MEK inhibitor RO4987655/CH4987655 (Hoffmann-La Roche/Chugai Pharmaceutical, Tokyo, Japan) is an orally active small molecule targeting mitogen-activated protein kinase (MAP2K or MEK) with potent anti-tumor activity [25]. RO4987655 binds to and inhibits MEK1, which results in the inhibition of MEK-dependent cell signaling and tumor cell proliferation. A phase I study of RO4987655 demonstrated its promising anti-tumor activity, which was further investigated in specific populations of patients with RAS and/or RAF mutation-driven tumors. [^{18}F] FDG-PET imaging was included in the clinical efficacy assessments. Reduction in tumor [^{18}F] FDG uptake between baseline and day 15 was observed in 79.4% of patients with advanced solid tumors [10].

To examine the molecular basis for using [^{18}F] FDG as a PD biomarker for an early response to MEK inhibition, we have here performed longitudinal [^{18}F] FDG-PET imaging of metabolic responses to RO4987655 therapy in human lung carcinoma xenografts. The expression levels of the glucose transporter (GLUT1) and the activity of hexokinase 1, which have been shown to be related to [^{18}F] FDG uptake in human cancer [26], were examined using semi-quantitative fluorescent immunohistochemistry (fIHC). RPPA was used to assess RO4987655 effects on the MAPK/PI3K pathway components in order to make correlations with the metabolic changes determined in the tumors by [^{18}F] FDG-PET.

Methods

Cell culture and reagents

The human lung adenocarcinoma cell line NCI-H2122 was purchased from the American Type Culture Collection (ATCC). All cells were maintained in the designated media and indicated concentrations of heat-inactivated fetal bovine serum (Gibco, Langley, OK, USA) and L-glutamine (Sigma, St. Louis, MO, USA) according to the ATCC recommendations. Cells were grown at 37°C

in an atmosphere of 5%CO_2. RO4987655 (CH4987655), 3,4-difluoro-2-(2-fluoro-4-iodophenylamino)-5-(3-oxo-1,2-oxazinan-2-ylmethyl)benzohydroxamic acid 2-hydroxyethyl ester, was synthesized by Chugai Pharmaceuticals Co., Ltd. The RO4987655 chemical structure is provided in Additional file 1. For *in vivo* use, the drug was dissolved in 50% ethanol/50% Cremophor® EL (Sigma) and stored at −20°C. The vehicle and RO4987655 stock solutions for *in vivo* experiments were diluted fivefold with distilled water on each dosing day.

Cell proliferation and assay and Western blotting

Cells were treated with various concentrations of RO4987655 for 72 h in 96-well plates and viable cells were quantified with Cell Counting Kit-8 (Dojindo Molecular Technologies, Inc, Rockville, MD, USA). For Western blotting, cells were treated with RO4987655 for indicated periods and lysed with cell lysis buffer (Cell Signaling Technology, Beverly, MA, USA) containing a protease inhibitor cocktail (cOmplete, EDTA-free, Roche, Deutschland, Germany), phosphatase inhibitor cocktails 2 and 3 (Sigma), and 1 mM PMSF (Sigma). For detection of protein bands, the following were used as primary antibodies: pEGFR (Y1068, Cell Signaling Technology, 20234S), EGFR (Cell Signaling Technology, 20234S), pMKK4 (S257/T261, Cell Signaling Technology, #9156), MKK4 (SEK1(5C10), Cell Signaling Technology, #3346), pAKT (S473, Cell Signaling Technology, 9271), AKT (Cell Signaling Technology, 9272), pERK (T202/Y204, Cell Signaling Technology, 9101), ERK (Cell Signaling Technology, 9102), pMEK1/2 (S217/S221, Cell Signaling Technology, 9121), MEK (Cell Signaling Technology, 9122), Cyclin D1 (NeoMarkers, RB-010-P0), and actin (Santa Cruz, sc-1616). All protein bands were visualized with secondary antibodies labeled with HRP and ECL system (GE Healthcare, Wilmington, MA, USA) by using ImageQuant LAS 4000 (GE Healthcare).

Synthesis of [^{18}F] FDG

[^{18}F] FDG was obtained as an aliquot from daily clinical production at the Karolinska University Hospital and was subjected to all quality tests performed for administration in humans. Identity and radiochemical purity were determined using radio-thin layer chromatography and radio-liquid chromatography analyses prior to release.

Xenograft tumor models

Female athymic nude mice Balb nu/nu, age 5 to 6 weeks (18 to 22 g) were purchased from NOVA/SCB (Sollentuna, Sweden) and Charles River Lab International, Inc. (New York, NY, USA). Animal care, handling, and health monitoring were carried out in accordance with the Guidelines for Accommodation and Care of Laboratory Animals. All animal experiments were performed in accordance with protocols approved by the institutional animal care committee. NCI-H2122 cells (4×10^6/mouse) were inoculated subcutaneously in the right flank of Balb-nu/nu mice. Once tumors were established (100 to 200 mm^3), mice were randomized into groups with similar mean tumor volumes at the start of the study. Tumor volume and body weight were measured on days 0 (baseline), 1, 2, 3, and 9 of [^{18}F] FDG-PET imaging. Tumor growth inhibition was calculated using the following formula: TGI = $[1 - (T - T_0) / (C - C_0)] \times 100$, where T and T_0 are the mean tumor volumes on specific experimental day and on the first day of the treatment, respectively, for the experimental groups and likewise, where C and C_0 are the mean tumor volumes for the control groups. The daily administration was selected on preliminary screening studies and was lower than the maximal tolerated dose (MTD), defined as the maximum dose associated with <20% weight loss and no toxic deaths.

PET imaging

Further details on the PET imaging are provided in Additional file 2. A time interval of 20 to 24 h was used between daily RO4987655 administration and completion of PET imaging for each tumor-bearing mouse and for each PET imaging time point (day 0, 1, 3 and 9). Mice were fasted for 6 to 8 h prior to start of the imaging session. [^{18}F] FDG (7 to 8 MBq per mouse, maximum volume of 200 μL) was administered to awake, warmed (37°C) mice by a bolus injection via the tail vein. Forty to sixty minutes after the tracer injection, the mice were administered with isoflurane, controlled by an E-Z anesthesia vaporizer (5% initially and then 1.5% to maintain anesthesia, blended with 7:3 air/O_2 and delivered through a Microflex non-rebreathing mask from Euthanex Corporation, Palmer, PA, USA). The mice were placed on a heated pad (37°C) on the camera bed, with most of the body volume in the field of view (7.68 cm). Emission data were collected for 20 min in list mode with a microPET Focus 120 scanner (CTI Concorde Microsystems). Maximum standardized uptake values (SUV_{max}) of [^{18}F] FDG uptake in the tumor were calculated and normalized to the administered activity (MBq/body weight, g). The drug effect on tumor metabolism was estimated as%SUV_{max} change to day 0 (baseline).

Fluorescent immunohistochemistry (fIHC)

Further details on the fluorescent immunohistochemistry (fIHC) are provided in Additional file 2. Tumors were collected for fIHC analyses 20–22 h after daily RO4987655 administration for each [^{18}F] FDG-PET time point (days 0, 1, 3 and 9). For fIHC, tumor samples were fixed by immersion for 24 h in a solution of 4% paraformaldehyde in 0.1 M phosphate buffer (pH 7.4) containing phosphatase inhibitors. Tissue blocks containing 4 to5 tumor samples of different treatment groups were

snap frozen, cryosectioned at 14-μm thickness, and thaw-mounted on Superfrost Plus slides. Single- and multi-labeling experiments were performed as described previously [27]. Briefly, sections were incubated with rabbit anti-GLUT1 (Abcam, AB653, dilution 1:300) and anti-hexokinase 1 (Abcam, AB65069, dilution 1:200) antibodies and were visualized by incubation with Alexa488 conjugated donkey anti-rabbit antibody. Whole slide images were captured on a Metasystems Vslide system (Newton, MA, USA) equipped with appropriate filter sets using a × 10 objective. Channel grey scale images were analyzed using ImageJ software (1.45p NIH, Bethesda, MD, USA) and GLUT1 and hexokinase 1 fluorescence intensity were measured from 50 randomly selected spots within each tumor sample. Supporting quantification figure is available as an additional information (Additional file 3).

Reverse phase protein arrays

Tumors were collected for RPPA analyses 20 to 22 h after daily RO4987655 administration for each [^{18}F] FDG-PET time point (days 0, 1, 3, and 9). Histological examination of 15-μm thick frozen sections revealed good morphology of tissues, with 75% to 90% vital tumor content (10% to 25% fibrosis, no necrosis). Tumor extracts of all samples were prepared using 100 μL of lysis buffer CLB1 for 30 min at room temperature. Protein concentrations of lysates were determined by Bradford Assay (Coomassie Plus-The better Bradford™ Assay, Thermo Scientific, Waltham, MA, USA). For the production of RPPA chips, the tumor lysates were adjusted to 3 mg/ml protein concentration in CLB1 buffer and subsequently diluted tenfold with printing buffer CSBL1. The lysates were printed onto Zeptosens chips (Bayer Technology Services GmbH, Leverkusen, Germany) using a Gesim NP2.0 Nanoplotter (GeSiM, Grosserkmannsdorf, Germany) and single droplet deposition of lysate (0.4 nL per sample spot). Lysate samples were printed at four serial dilutions (start concentration 0.3 mg/mL, plus 1.6-fold dilutions), each dilution as duplicate spots (in total eight spots per sample). Array images and data were analyzed with the software ZeptoVIEW 3.1 (Zeptosens, Witterswil, Switzerland).

The list of signaling proteins representing MAPK/PI3K/glycolic pathways and included in the RPPA analyses is provided in Additional file 4 for day 1 and in Additional file 5 for day 3 of the RO4987655 treatment. RPPA analyses were performed at the NMI Natural and Medical Sciences Institute, Reutlingen, Germany. The Ingenuity pathway analysis, a web-based software application, was used for comparison of MAPK/PI3K pathway modulations on days 1 and 3 of RO4987655 treatment.

Statistical analysis

For the comparison of [^{18}F] FDG-PET data, a pair-wise *t* test with Tukey-Kramer correction for multiple testing was applied using the software JMP (Version 10, © 2012 SAS Institute Inc., Cary, NC, USA). For the analysis of the relationship of dose level and biomarker data from both RPPA and fIHC, a statistical model based on a least squares fit including the factors dose and dose^2 was implemented using the software JMP (Version 10, © 2012 SAS Institute Inc.).

Results

In vitro effects of RO4987655 on MAPK/AKT pathway components in NCI-H2122 cells

Prior to *in vivo* studies, the efficacy of the RO4987655 treatment against NCI-H2122 cells was tested *in vitro*. RO4987655 at doses ranging from 0.1 to 1.0 μM suppressed pERK1/2 already at 2 h after the start of treatment. Modest increases of pMEK and pAKT levels were observed at this time point (Figure 1a). The drug treatment over the time course at 0.1 μM of RO4987655 demonstrated transient decreases in pERK1/2, pMKK4, and cyclin D1 expressions on day 1, followed by their slight up-regulation on day 3. Since RO4987655 is a selective MEK inhibitor [25], it had no influence on pEGFR and pMEK at 6 h after the drug treatment, but, similar to pERK1/2, pMKK4, and cyclin D1, pEGFR and pMEK were up-regulated on day 3 (Figure 1b). This up-regulation is known as a feedback reactivation of MAPK pathway by selective MEK inhibitors in *K-ras*-mutated cells [28]. Consistent with this signal blocking property in NCI-H2122 cells, RO4987655 inhibited proliferation of NCI-H2122 cells in a dose-dependent manner with an IC_{50} value of 0.0065 μM (Figure 1c).

[^{18}F] FDG-PET imaging in NCI-H2122 tumor xenografts, harboring *K-ras* mutation, during RO4987655 treatment

The [^{18}F] FDG-PET imaging studies in NCI-H2122 tumor xenografts consisted of two experiments: the dose-ranging (1.0 to 5.0 mg/kg) studies with imaging on days 0, 1, and 3 of treatment and the time course study of serial [^{18}F] FDG-PET scans at baseline and 2 h as well as days 1, 3, and 9 of treatment with 2.5 mg/kg of RO4987655.

We first aimed to determine the earliest time-point of the RO4987655 treatment response, detectable by [^{18}F] FDG-PET. Once tumor xenografts were established, mice were randomized into study groups and the treatment was initiated. The tumors size was estimated with digital caliper and PET scans performed on days 0, 1, and 3 with 1.0, 2.5, and 5.0 mg/kg RO4987655. The vehicle treatment did not inhibit the NCI-H2122 tumor xenograft growth over this time frame. In contrast, RO4987655 treatment resulted in 119% tumor growth inhibition (TGI) at 1.0 mg/kg, 145% TGI at 2.5 mg/kg and 150% TGI at 5.0 mg/kg on day 3 (Figure 2a). PET imaging showed that [^{18}F] FDG uptake in the xenografts decreased within 24 h (day 1) from the administration of

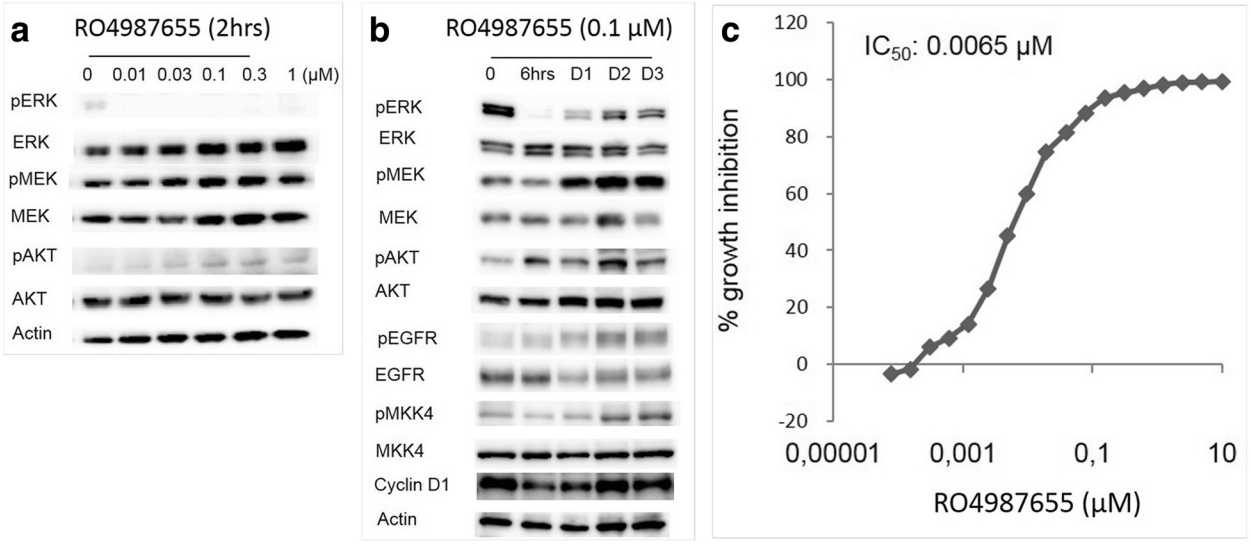

Figure 1 In vitro RO4987655 effects on MAPK/PI3K pathway in NCI-H2122 (*K-ras*) cells. (a) The cells were treated with indicated concentrations of RO4987655 for 2 h. Cell lysates were analyzed by immunoblotting with antibodies to the phosphorylated versus total ERK1/2, MEK1/2, and AKT. Actin was used as a loading control. **(b)** Time-dependent biomarker responses of NCI-H2122 cells to RO4987655 inhibition (0.1 μM). **(c)** Dose-dependent anti-proliferative inhibition of RO4987655 in cells yielding a 50% inhibitory concentration (IC_{50}) of 0.0065 μM.

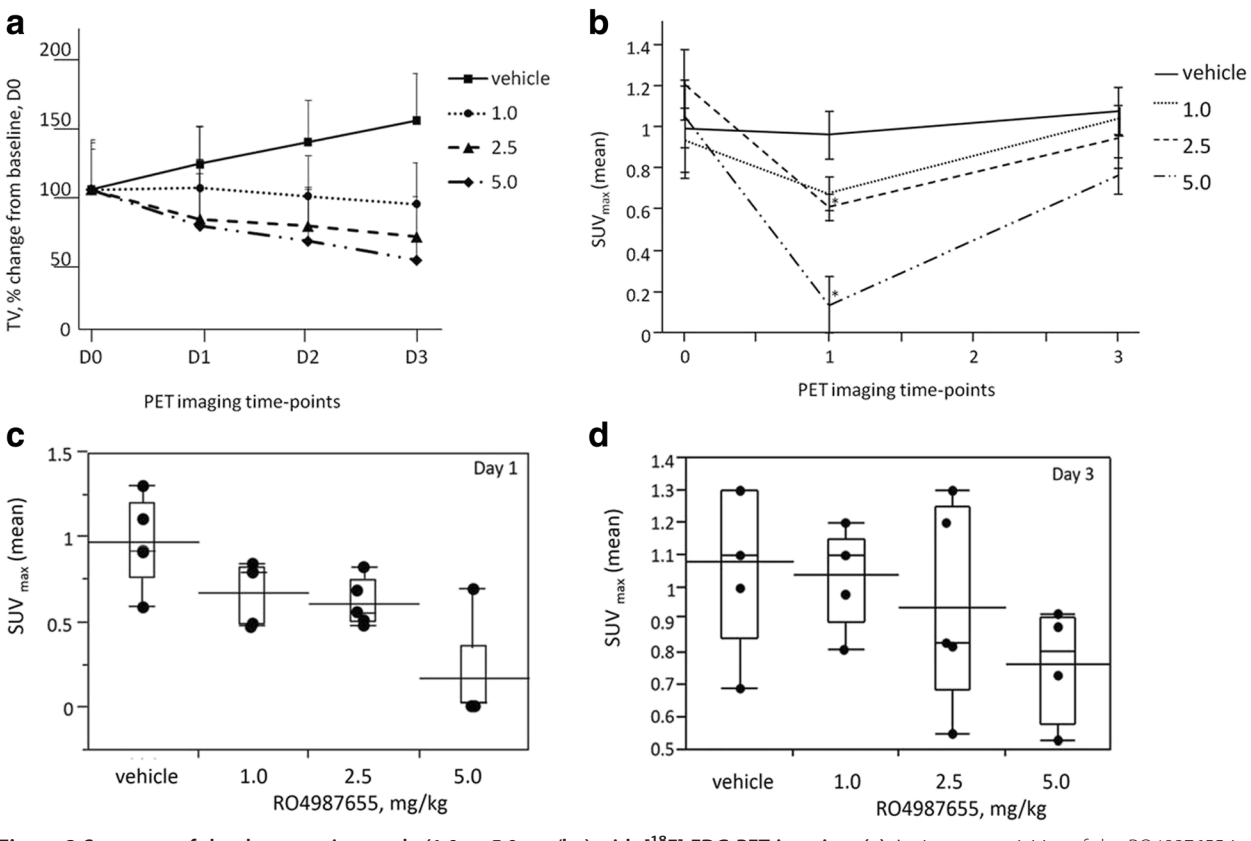

Figure 2 Summary of the dose-ranging study (1.0 to 5.0 mg/kg) with [^{18}F] FDG-PET imaging. (a) Anti-tumor activities of the RO4987655 in NCI-H2122 tumor xenografted mice on days 0, 1 and 3 of the treatment. **(b)** Dose-and time-dependent FDG tumor uptake from day 0 (baseline) to day 3 of the treatment. Analysis of SUV_{max} values between dose groups on day 1 **(c)** and day 3 **(d)** of the treatment.

RO4987655. However, this decrease was followed by a time- and dose-dependent rebound in uptake from day 1 to day 3, even though tumor growth inhibition continued on day 3 of the treatment (Figure 2b).

The PET data were analyzed for significant differences between dose groups. On day 1 of the treatment, the 5.0 mg/kg group showed significantly lower [^{18}F] FDG uptake ($^*p = 0.0002$) than that of the vehicle and 2.5 and 1.0 mg/kg groups ($^*p = 0.0253$ and $^*p = 0.0103$, respectively) by a pairwise t test (Figure 2c). There were no significant differences for SUV_{max} among the three dose groups on day 3 ($p = 0.24$) (Figure 2d). After the last PET scans, on day 3 of the treatment, the mice were sacrificed and tumors were resected for further analyses.

Figure 3 (the upper panel) demonstrates representative maximum intensity projection (MIP) PET images of nude mice bearing NCI-H2122 tumor xenografts, scanned on days 0, 1, and 3 after the treatment with vehicle (Figure 3a) and RO4987655, 5.0 mg/kg (Figure 3c). The lower panel shows corresponding transverse sections through a plane of the mouse body that includes tumor (T) on days 0, 1, and 3 after vehicle (Figure 3b) and RO4987655 (5.0 mg/kg) (Figure 3d) treatment.

Our previous experiments with FDG distribution kinetics in Balb nu/nu mice demonstrated that tracer accumulation in tumors reached its plateau in approximately 40 min after the tracer injection. Therefore, in this study, PET scans were performed 40 to 50 min after the FDG injection. The mice were physically active during FDG accumulation period (40 to 50 min) before PET imaging; therefore, physiological FDG uptake in brain, brown fat, and muscles was observed on PET images, and tumors were clearly distinct from surrounding tissues.

To extend the previous dose-ranging PET imaging experiments, we added an acute (2 h post-treatment) and a late (9 days after the treatment) [^{18}F] FDG scan, in addition to baseline, days 1 and 3 time points (six animals per group at each time point) after single administration of 2.5 mg/kg RO4987655 to NCI-H2122 xenografted mice. In the dose-ranging study, treatment with RO4987655 5.0 mg/kg led to dramatic decrease in FDG uptake on day 1 (Figure 3d) that caused difficulties with tumor delineation on PET images. Therefore, for the time course study, the RO4987655 dose of 2.5 mg/kg was chosen.

Figure 4a demonstrates an example of one-mouse follow-up [^{18}F] FDG-PET MIP images, performed at day 0 (baseline), 2 h, days 1, 3, and 9 after treatment with RO4987655. Tumor locations are indicated with white circles. Figure 4b shows corresponding transverse sections through a plane of the mouse body that includes tumor (T).

The TGI results were similar to those obtained in the dose-ranging studies, including treatment days 1 and 3. Tumor volumes remained comparable between days 3 and 9 (Figure 4c). At the same time, we observed a decrease in [^{18}F] FDG uptake in the tumors (15.4% change compared to baseline) as early as 2 h after the start of treatment. We continued with the daily RO4987655, 2.5 mg/kg treatment followed by PET examinations on days 1, 3, and 9 of the drug administration. The maximum decrease was observed on day 1 (44% change, with statistically significant differences compared to baseline ($^*p < 0.05$)), followed by a slight rebound on day 3 (33.6% change, $^*p < 0.05$). The effect plateaued thereafter to day 9 of treatment. Serum glucose levels remained comparable over these times (data not shown).

Fluorescence immunohistochemistry

In order to investigate the mechanism of the PET rebound on day 3, we measured the status of molecular markers in the xenografts. Levels of the [^{18}F] FDG uptake markers,

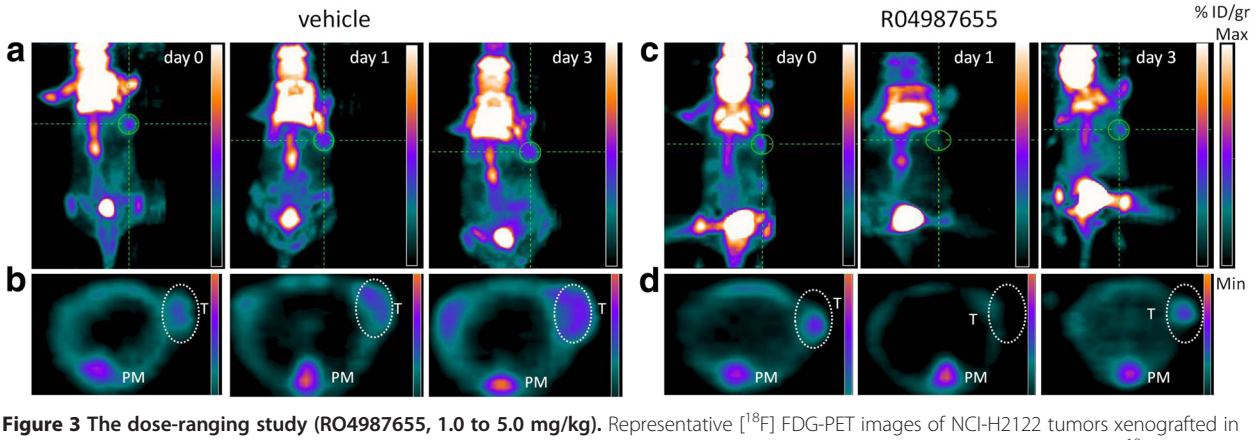

Figure 3 The dose-ranging study (RO4987655, 1.0 to 5.0 mg/kg). Representative [^{18}F] FDG-PET images of NCI-H2122 tumors xenografted in Balb nu/nu mice, treated with vehicle and RO4987655 and scanned on days 0, 1 and 3 after treatment. The one-mouse follow-up [^{18}F] FDG-PET MIP images (upper panel) and corresponding transaxial sections (lower panel) performed on days 0, 1, and 3 after vehicle **(a, b)** and RO4987655, 5.0 mg/kg treatment **(c, d)**. The transaxial tumor sections **(b, d)** show a plane of the mouse body that includes tumor (T). The same color scale was applied to all FDG-PET images after correction for injected dose per gram tissue,% ID/gr, to show the relative [^{18}F] FDG uptake in the tissues.

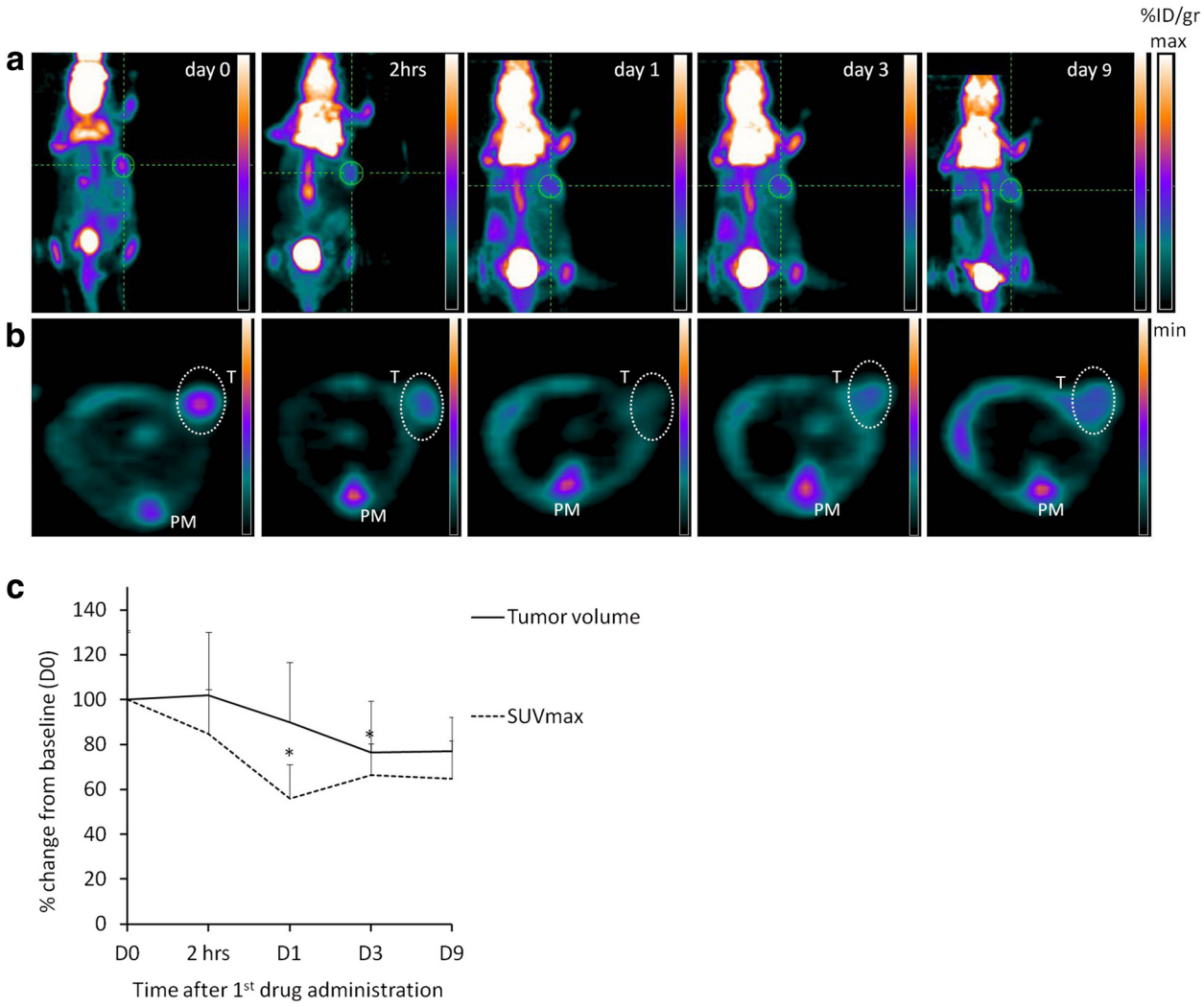

Figure 4 Summary of the time course study of serial [^{18}F] FDG-PET imaging. (a) Representative one-mouse follow-up [^{18}F] FDG-PET images, performed at day 0 (baseline), 2 h, days 1, 3, and 9 after treatment with RO4987655, 2.5 mg/kg Tumor locations are indicated with the white circle. **(b)** Corresponding transverse sections through a plane of the mouse body that includes tumor (T); PM, paraspinal muscle. **(c)** Comparison of RO4987655, 2.5 mg/kg anti-tumor activities, and FDG-PET imaging results in NCI-H2122 tumor xenografted mice on day 0, after 2 h and days 1, 3, and 9 of the treatment (*$p < 0.05$, compared to baseline, day 0). The same color scale was applied to all FDG-PET images after correction for injected dose per gram tissue,% ID/gr, to show the relative [^{18}F] FDG uptake in the tissues.

hexokinase 1 and GLUT1, in the resected xenograft tumors were visualized using immunofluorescence. Five slides each containing 4 to 5 tumor samples of different treatment groups (22 samples) were stained simultaneously and whole slides were scanned using × 10 primary objective. Antibodies against hexokinase 1 and GLUT1 only labeled tumor cells and immunoreactivity could not be detected in connective tissue (Figure 5a1 to a5 and 5c1 to c5). Hexokinase 1 immunoreactivity showed large variability within (core versus periphery) and among tumor samples (data not shown). A comparison of average fluorescence intensity revealed modest increases in hexokinase 1 activity on day 3 of the RO4987655 treatment, although the changes were not statistically significant in any of the treatment groups compared to untreated controls (Figure 5b). Inter-tumor variability for GLUT1 immunoreactivity was much lower compared to hexokinase 1 levels. Analysis of average GLUT1 immunoreactivity revealed a gradual decrease in GLUT1 levels reaching significance after 3 days treatment with a RO4987655 dose of 5 mg/kg (Figure 5d).

In vivo effects of RO4987655 on MAPK/PI3K pathway components assessed by RPPA

Responses of MAPK/PI3K/glycolytic signal transduction pathways to RO4987655 inhibition (doses ranging from

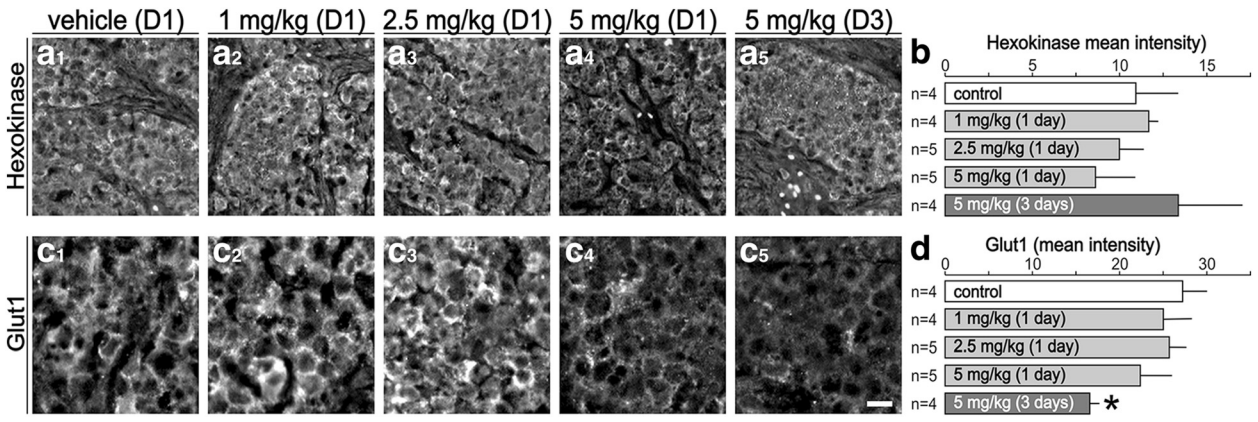

Figure 5 Fluorescence immunohistochemistry results. Immunofluorescence micrographs, showing the distribution of hexokinase 1 **(a1 to a5)** and GLUT1 **(c1 to c5)**. Comparison of average fluorescence intensities in hexokinase 1 levels **(b)** and GLUT 1 expressions **(d)** among the RO4987655 dose groups.

1.0 to 5.0 mg/kg) were analyzed in the tumors collected on days 1 and 3 of the treatment after PET imaging. The tumors were resected immediately after PET scans (approximately 20 to 22 h after drug administration). We found that 11 (Table 1) out of 50 investigated protein markers (Additional file 4) analyzed on days 1 and 10 (Table 2) out of 83 investigated protein markers (Additional file 5) analyzed on day 3 of the RO4987655 treatment revealed significant dose-dependent modulations. The Ingenuity Pathway Analysis (IPA) software was used for mapping MAPK/PI3K pathways cascade phosphoproteins significantly modulated on day 1 (Figure 6a) and day 3 (Figure 6b) of the treatment.

RPPA analysis showed dose-dependent modulations of pERK1/2, pMKK4, and pEGFR with a strong reduction in phosphorylated levels both on days 1 and 3 of the treatment. In addition, after 1 day of treatment, MEK inhibition resulted in not only significant dose-dependent down-regulation of pmTOR (Table 1) but also up-regulation of pC-RAF and reactivation of pMEK1/2, pMEK2, and pAKT on day 3 of the treatment (Table 2). Cyclin D1 showed enhanced expressions on both treatment days (Figure 7). pAKT and pMEK2 were also up-regulated on day 1. However, this regulation was statistically significant only on day 3 of the treatment.

Table 1 The RPPA markers that showed significant modulations after 1 day of the RO4987655 treatment

Analyte	*P* value	Pathway
	Down-regulated	
ERK1/2-P-Thr201/Tyr204	<0.001	MAPK
PKC alpha/beta II-P-Thr638/641	<0.001	cAMP/metabolism
MKK4-P-Ser257/Thr261	<0.001	MAPK
mTOR-P-Ser2448	0.005	mTOR
EGFR-P-Tyr1068	0.0039	RTK
PKA C-alpha/beta/gamma-P-Thr197	0.0049	c/AMP/metabolism
GSK3 beta-P-Ser9	0.0267	Wnt/metabolism
MEK1/2-P-Ser217/221	0.00267	MAPK
	Up-regulated	
IGF-receptor	0.0034	Insulin
4E-BP1	0.0062	Metabolism
Cyclin D	0.0168	Cell cycle control
P53	0.0221	Cell cycle control
Akt-P-ser473	0.0991	Akt/metabolism
MEK2	0.6743	MAPK
C-met	0.8373	RTK

Discussion

We have recently reported the use of [^{18}F] FDG-PET as a PD biomarker for the efficacy of a first-in-class dual

Table 2 The RPPA markers that showed significant modulations after 3 days of the RO4987655 treatment

Analyte	*P* value	Pathway
	Down-regulated	
ERK1/2-P-Thr202/Tyr204-rbm	0.00001	MAPK
EGFR-P-Tyr1068	0.0058	RTK
MKK4-P-Ser257/Thr261	0.0483	MAPK
	Up-regulated	
MEK1/2-P-Ser217/221	0.00098	MAPK
Akt-P-Ser473	0.0034	Akt/metabolism
c-Met	0.0242	RTK
P53-P-Ser392	0.025	Cell cycle control
Cyclin D1	0.0302	Cell cycle control
C-Raf-P-Ser338	0.0371	MAPK
MEK2	0.0433	MAPK

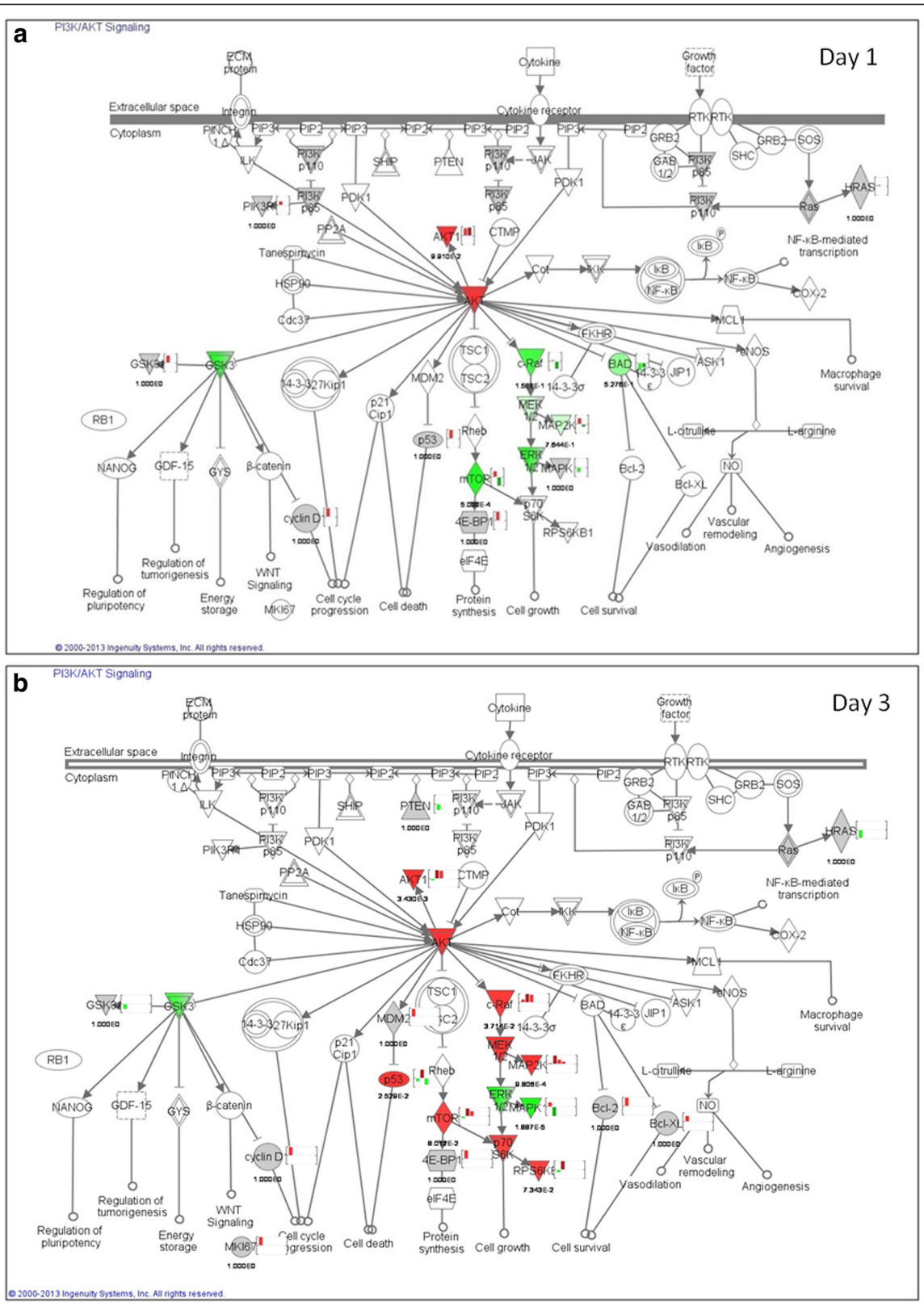

Figure 6 (See legend on next page.)

(See figure on previous page.)
Figure 6 Ingenuity pathway analysis of the RO4987655 treatment effects on regulation of MAPK/PI3K/AKT pathway phospho-proteins. **(a)** Day 1 and **(b)** day 3 of the treatment (colored markers for scores measured on the RPPA platform, green - negative and red - positive dose-related regulation). The first column in the bar chat represents the regulation of the total protein, the second column the regulation of the corresponding phospho-protein. In cases where more than one phospho sites were measured for the same protein, the third (and so forth) column represents the regulation for the second (and so forth) phospho-protein. The grey nodes represent proteins where only the total proteins were measured but no phosphorylated forms.

MEK/Raf inhibitor, RO5126766, in preclinical *K-ras* or *B-raf* mutant tumor xenografts models [16]. RO5126766 was designed to inhibit ERK signaling outputs more effectively than standard MEK inhibitors [28]. The preclinical [^{18}F] FDG-PET results in tumor xenografts were found to parallel the [^{18}F] FDG-PET results obtained in a phase I dose escalation study in humans [11]. The novel allosteric MEK inhibitor RO4987655 studied here binds and inhibits MEK, resulting in the suppression of MEK-dependent cell signaling [25]. Both RO5126766 and RO4987655 have been assessed with [^{18}F] FDG-PET in phase I dose-escalation clinical trials and have shown promising anti-tumor activities with strong decreases in tumor metabolic responses [10,11]. Interestingly, the [^{18}F] FDG-PET data collected during these independent studies led to different recommendations in the doses of RO5126766 and RO4987655 for phase II [29].

To investigate further whether preclinical [^{18}F] FDG-PET imaging would also mirror the clinical observations obtained for RO4987655, we performed longitudinal PET scans of metabolic responses in *K-ras*-mutated NCI-H2122 tumor xenografts in mice. Unlike the gradual reductions in tumor [^{18}F] FDG uptake by RO5126766 over the treatment time, RO4987655 induced significant decreases in tumor metabolic activities already by day 1. However, this decrease was followed by rapid dose-dependent rebounds in the [^{18}F] FDG uptake at day 3, even though the drug was administered daily. To investigate the mechanism for the [^{18}F] FDG-PET response despite continued TGI, we first examined whether the tumor metabolic feedback activation in response to MEK inhibition on day 3 correlated with GLUT1 and hexokinase 1, using semi-quantitative fIHC. We found that the increase in [^{18}F] FDG uptake on day 3 was associated with elevated hexokinase 1, which is consistent with studies reporting that increased levels of hexokinases enhance [^{18}F] FDG intracellular trapping [30,31]. Furthermore, our observation was in agreement with several other studies that have shown correlations of [^{18}F] FDG uptake and hexokinase expression in response to MEK inhibition [17]. However, the hexokinase changes observed here were not statistically significant nor did changes in GLUT1 transporter expression significantly correlate with the observed [^{18}F] FDG changes. These results are mostly likely due to the high intra- and inter-tumoral variability of GLUT1 and hexokinase 1 expression in our IHC. No other significant treatment effects were identifiable with this technique. Previous studies have demonstrated that correlations between GLUT expressions and hexokinase activities and [^{18}F] FDG uptake are more pronounced at the cellular level and have proposed that this could serve as a good *in vitro* screening for testing the feasibility of cells to be used in xenograft cancer models for PET imaging [16,32]. However, as discussed in [33-35] and also observed in our

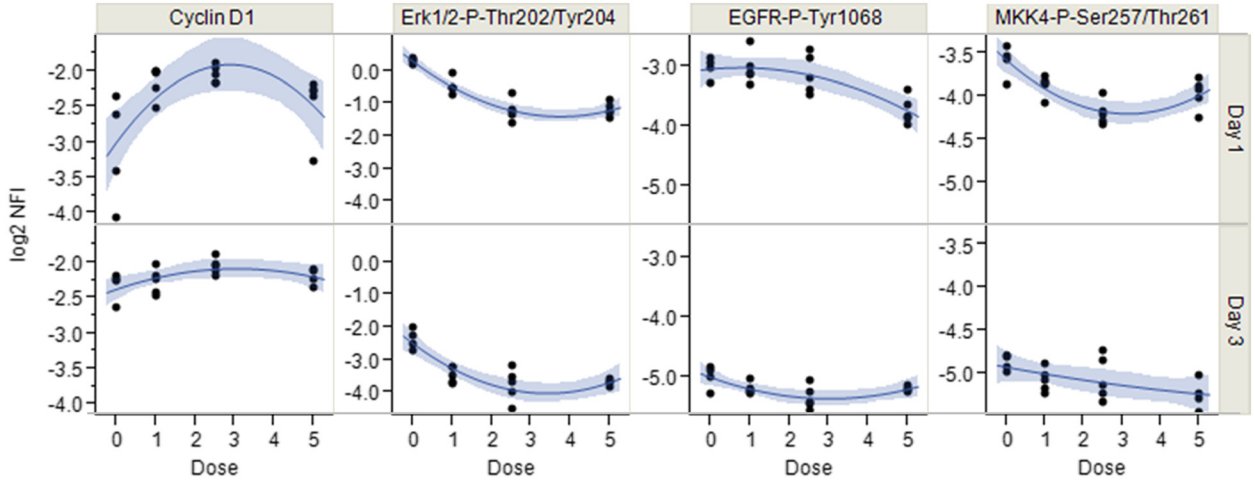

Figure 7 RPPA results. Four markers that showed a significant dose effect on both day 1 and day 3 are visualized showing the individual data points for different animals along with a quadratic fit and the corresponding confidence region.

study, these relationships *in vivo* were not as predictive as expected, most likely because [^{18}F] FDG uptake *in vivo* will depend on many factors: not only glucose transporters, hexokinases, and glucose-6-phosphatase activities but also the intra-tumoral cell density, blood supply, fraction of hypoxic tissue, and viable cell numbers.

We also analyzed the effect of RO4987655 on specific cellular signaling components. We showed *in vitro* (Figure 1) that RO4987655 decreased pERK1/2 activities in tumor cells followed by a pERK1/2 increase and up-regulated phosphorylation of MEK, MAP2K4 (MKK4), and EGFR at later time points. Also, a modest increase of pAKT, which is a component of the alternative PI3K pathway involved in cell survival signaling as well as glucose homeostasis regulation, was observed. These results might indicate that NCI-H2122 cells can be affected by a negative feedback upon the MEK kinase inhibition.

RPPA proteomics technology was used to investigate the molecular changes of the signaling status *in vivo* that would influence the [^{18}F] FDG uptake in NCI-H2122 tumors upon treatment since it permits multiplex, highly sensitive, and reproducible quantitative analysis of protein expression and phosphorylation levels. To our knowledge, there are no previous reports in the literature that have combined preclinical [^{18}F] FDG-PET with RPPA for evaluating MEK inhibition efficacy.

In the xenograft experiment at 1.0, 2.5, and 5.0 mg/kg, the significant pERK1/2 down-regulations revealed by RPPA, both on day 1 and day 3 in all dose groups, confirmed that this MEK inhibitor clearly hits its target in the xenografted tumors. These results support previous publications proposing the inhibition of ERK phosphorylation in tumors as a PD biomarker of MEK inhibition [28,36,37]. RPPA also revealed significant reductions of levels of pMKK4, a direct activator of MAP kinases in response to various environmental stresses of mitogenic stimuli [38], and of pEGFR, an upstream Ras activator, on both treatment days (Tables 1 and 2).

In a recently published study, MEK inhibition in cancers by RO4987655 was demonstrated by decreases in ERK1/2 phosphorylation [10]. Prior reports using RO4987655 with *B-raf*-mutated HT-29 human colon cancer xenografts also showed a marked reduction of pERK [25]. In addition, an apparent relationship between [^{18}F] FDG-PET data and the degree of pERK suppression by RO4987655 in peripheral blood mononuclear cells of melanoma patients was reported [29]. In this study, we observed different pERK1/2 responses on day 3 in the *in vivo* and *in vitro* settings. In our *in vitro* study at 0.1 μM of RO4987655, we observed pERK1/2 up-regulation after initial down-regulation. This is well known as a relief from a negative feedback on RAF by MEK inhibition and is apparently due to feedback regulation since there is no drug clearance. In contrast, in our *in vivo* study, as revealed by RPPA, pERK1/2 was clearly suppressed even on day 3 at all doses. In our previous study with *B-raf*-mutated HT-29 xenografts [25], tumor pERK1/2 returned to the basal level after 24 h from 6.25 mg/kg RO4987655 administration due to the clearance of the drug from blood in animals. In the current study, we administered the drug daily and we resected the tumors just after the drug administration. Therefore, pERK1/2 down-regulation was observed even at day 3.

We also observed an up-regulation of pC-Raf and pMEK1/2 on day 3 (Table 2), which is in agreement with other reports [39] in which MEK inhibition led to an increase in pMEK through feedback-mediated Ras activation. Interestingly, RO4987655 caused an activation of cyclin D1, which was observed as early as day 1 of the treatment. This increase can only be partly explained by an activation of alternative pathways since the reactivation of the MAPK pathway seems to be fully established at day 3 that is 2 days later than the up-regulation of cyclin D1 could be observed. As described by Rexer et al. [40], the activation of alternative PI3K/AKT pathways limits the anti-tumor activity of MEK inhibitors and down-regulation of cyclin D1 or reduced tumor cell proliferation is not necessarily expected. Increased cyclin D1 expression in cells that showed resistance to MAPK inhibitors has been reported [41]. Thus, the activation of cyclin D1 during the RO4987655 treatment may limit the inhibitory effects of MEK inhibition on tumor growth.

In addition, as described above, the current study found significantly increased phosphorylation of AKT on day 3 of the RO4987655 treatment. Up-regulation of pAKT may lead to the activation of the downstream signals that regulate glucose metabolism and cell survival. Thus, there are two potential implications of the [^{18}F] FDG-PET rebound on day 3 of RO4987655 treatment: up-regulating glucose uptake by activating AKT signal and/or stimulating cell growth by reactivating the ERK/MAPK pathway signal.

Concerning the direct up-regulation of glucose uptake by activating AKT signaling, our initial investigation of the expression levels of GLUT1 and hexokinase 1 in the tumors with fIHC failed to identify any statistically significant correlations between the [^{18}F] FDG-PET rebound and protein expression. The expression profiling of these proteins as well as other GLUT-family members (for example, GLUT3) and hexokinase 2 in combination with a more accurate quantitative approach needs to be undertaken to clearly understand the correlations between [^{18}F] FDG uptake and AKT signal activation by MEK inhibition in *K-ras*-mutated tumors.

Concerning the indirect up-regulation of glucose uptake by stimulating cell survival via AKT signaling, we hypothesize that the rebound effect in response to MEK inhibition by RO4987655 seen in the [^{18}F] FDG-PET analysis is due to activation of the PI3K/AKT mediated

cell survival pathway. This is supported by studies with other MEK inhibitors, such as AZD6244 and HER2-driven cancers [42], PD325901 in prostate cancer xenografts [43], and U0126 in a Wilms tumor model in mice [44]. Interestingly, it was shown that dual blockage of the compensatory PI3K/AKT/mTOR and RAS/MEK/ERK pathways can synergistically inhibit tumor cell growth *in vitro* and *in vivo* in different cancers [45-47]; combination treatment with MEK inhibitor AZD6244 and AKT inhibitor MK2206 was more effective than each drug alone in lung cancer patients [48].

An indirect up-regulation of glucose uptake by stimulating cell growth via reactivated ERK signaling is supported by a recent study with CH5126766 [28]. An enormous suppression of ERK signal achieved maximal tumor growth inhibition in both *B-raf* and *K-ras* xenograft models. Thus, reactivation of ERK signal by relief from the negative feedback to RAF may limit the anti-tumor activity as well as [^{18}F] FDG uptake at later time points.

These results are important for the use of [^{18}F] FDG-PET imaging in clinical drug development and for understanding the mechanisms behind changes in [^{18}F] FDG uptake induced by MEK inhibitors. In a clinical setting, a similar rebound in [^{18}F] FDG uptake observed in patients treated with MEK inhibitors may be useful for detecting the development of drug resistance long before increases in tumor size become detectable.

Conclusions

In this study, we have performed the first preclinical evaluation of MEK efficacy in *K-ras*-mutated tumor xenografts using a combination of molecular proteomics and non-invasive [^{18}F] FDG-PET imaging. The present study demonstrates the following:

- [^{18}F] FDG-PET revealed early transient metabolic suppression in the tumors in response to RO4987655
- MEK inhibition resulted in consistent pERK1/2 down-regulation in xenografts at all dose levels as observed by RPPA
- Modulation of molecular markers such as pMEK1/2, pC-Raf, pMKK4, pmTOR and pAKT suggested re-activation of the MAPK pathway as well as activation of the compensatory PI3K pathway, respectively. This may be causing the rebound in FDG uptake observed following treatment with RO4987655

The results obtained provide a strong rationale for combining RO4987655 with compounds affecting the PI3K/AKT pathway in order to overcome adaptive mechanisms of tumor resistance to MEK inhibition.

Additional files

Additional file 1: The RO4987655 chemical structure.

Additional file 2: An additional information to 'Methods' section.

Additional file 3: The supporting IHC quantification figure.

Additional file 4: List of 50 signaling proteins representing MAPK/PI3K/glycolic pathway and included in the RPPA analysis of tumors after one day of the RO4987655 treatment.

Additional file 5: List of 83 signaling proteins representing MAPK/PI3K/glycolic pathway and included in the RPPA analysis of tumors after three days of the RO4987655 treatment.

Abbreviations

[^{18}F] FDG-PET: fluorine-18-labeled glucose analog 2-fluoro-2-deoxy-D-glucose-positron emission tomography; ERK: extracellular signal-regulated kinase; fIHC: fluorescent immunohistochemistry; MEK (MAPK2): mitogen-activated protein kinase kinase; RPPA: reverse phase protein array analysis.

Competing interests

The authors declare that they have no competing interests.

Authors' contributions

TT, LL, and SSE designed and carried out the FDG-PET imaging, data acquisition, and analysis; TT and SSE drafted the manuscript. NM and JM performed immunohistochemical studies and statistical analysis; MV contributed to the concept of the paper and the selection of the technical platform (for RPPAs). ER, MV, and MP designed the RPPA studies and carried out RPPA analyses and helped in interpreting the RPPA data. SB and CHO performed the statistical and bioinformatics analysis. JT and VM were involved in planning, designing, and interpretation of the FDG-PET imaging studies. NI, SA, and YY designed and carried out the efficacy studies. NI also supported interpreting the data and drafting the manuscript. All authors read and approved the final manuscript.

Acknowledgements

The authors thank Berthold Gierke and Ewa Breitinger (NMI Natural and Medical Sciences Institute, Reutlingen) for performing the RPPA analyses, and Yasue Nagata (Chugai Pharmaceutical) for technical assistance on *in vitro* signal analysis. This project was performed in the framework of the Roche Postdoc Fellowship Program and was mentored and financially supported by Hoffmann-La-Roche. Additional financial support from the Karolinska Institutet, Swedish Research Council, the Swedish Governmental Agency for Innovation Systems, and the Swedish Foundation for Strategic research is gratefully acknowledged. The authors thank the production unit of the Neuroradiology Department at the Karolinska University Hospital for the delivery of [^{18}F] FDG and the staff of the Department of Comparative Medicine for skilled assistance and advice in the animal handling.

Author details

[1]Karolinska Institutet and Department of Neuroradiology, R3:00, MicroPET and Clinical Neurosciences, Karolinska University Hospital, Stockholm 17176, Sweden. [2]Pharmaceutical Research and Early Development (pRED), Oncology, Roche Diagnostics GmbH, Nonnenwald 2, Penzberg 82377, Germany. [3]Pharmaceutical Research and Early Development (pRED), Pharmaceutical Sciences, Roche Diagnostics GmbH, Nonnenwald 2, Penzberg 82377, Germany. [4]Research Division, Chugai Pharmaceutical Co., Ltd., 200 Kajiwara, Kamakura 247-8530, Japan. [5]F. Hoffmann-La-Roche Ltd., Building 682/226, Steinentorberg 8/12, Basel 4070, Switzerland. [6]Karolinska Institutet, Science for Life Lab, Tomtebodavägen 23A, Solna 17176, Sweden. [7]Department of Biochemistry and Protein Profiling, NMI Natural and Medical Sciences Institute at the University of Tuebingen, Markwiesenstrasse 55, Reutlingen 72770, Germany.

Received: 21 March 2014 Accepted: 22 June 2014
Published online: 09 September 2014

References

1. Friday BB, Adjei AA: **Advances in targeting the Ras/Raf/MEK/Erk mitogen-activated protein kinase cascade with MEK inhibitors for cancer therapy.** *Clin Cancer Res* 2008, **14**:342–346.

2. Pratilas CA, Solit DB: **Targeting the mitogen-activated protein kinase pathway: physiological feedback and drug response.** *Clin Cancer Res* 2010, **16:**3329–3334.
3. Roberts PJ, Der CJ: **Targeting the Raf-MEK-ERK mitogen-activated protein kinase cascade for the treatment of cancer.** *Oncogene* 2007, **26:**3291–3310.
4. Fremin C, Meloche S: **From basic research to clinical development of MEK1/2 inhibitors for cancer therapy.** *J Hematol Oncol* 2010, **3:**8.
5. Schelling M, Avril N, Nahrig J, Kuhn W, Romer W, Sattler D, Werner M, Dose J, Janicke F, Graeff H, Schwaiger M: **Positron emission tomography using [(18) F] Fluorodeoxyglucose for monitoring primary chemotherapy in breast cancer.** *J Clin Oncol* 2000, **18:**1689–1695.
6. Weber WA, Petersen V, Schmidt B, Tyndale-Hines L, Link T, Peschel C, Schwaiger M: **Positron emission tomography in non-small-cell lung cancer: prediction of response to chemotherapy by quantitative assessment of glucose use.** *J Clin Oncol* 2003, **21:**2651–2657.
7. Spaepen K, Stroobants S, Verhoef G, Mortelmans L: **Positron emission tomography with [(18)F] FDG for therapy response monitoring in lymphoma patients.** *Eur J Nucl Med Mol Imaging* 2003, **30**(Suppl 1):S97–105.
8. Stroobants S, Goeminne J, Seegers M, Dimitrijevic S, Dupont P, Nuyts J, Martens M, van den Borne B, Cole P, Sciot R, Dumez H, Silberman S, Mortelmans L, van Oosterom A: **18FDG-Positron emission tomography for the early prediction of response in advanced soft tissue sarcoma treated with imatinib mesylate (Glivec).** *Eur J Cancer* 2003, **39:**2012–2020.
9. Flaherty KT, Puzanov I, Kim KB, Ribas A, McArthur GA, Sosman JA, O'Dwyer PJ, Lee RJ, Grippo JF, Nolop K, Chapman PB: **Inhibition of mutated, activated BRAF in metastatic melanoma.** *N Engl J Med* 2010, **363:**809–819.
10. Leijen S, Middleton MR, Tresca P, Kraeber-Bodere F, Dieras V, Scheulen ME, Gupta A, Lopez-Valverde V, Xu ZX, Rueger R, Tessier JJ, Shochat E, Blotner S, Naegelen VM, Schellens JH, Eberhardt WE: **Phase I dose-escalation study of the safety, pharmacokinetics, and pharmacodynamics of the MEK inhibitor RO4987655 (CH4987655) in patients with advanced solid tumors.** *Clin Cancer Res* 2012, **18:**4794–4805.
11. Martinez-Garcia M, Banerji U, Albanell J, Bahleda R, Dolly S, Kraeber-Bodere F, Rojo F, Routier E, Guarin E, Xu ZX, Rueger R, Tessier JJ, Shochat E, Blotner S, Naegelen VM, Soria JC: **First-in-human, phase I dose-escalation study of the safety, pharmacokinetics, and pharmacodynamics of RO5126766, a first-in-class dual MEK/RAF inhibitor in patients with solid tumors.** *Clin Cancer Res* 2012, **18:**4806–4819.
12. Infante JR, Fecher LA, Falchook GS, Nallapareddy S, Gordon MS, Becerra C, DeMarini DJ, Cox DS, Xu Y, Morris SR, Peddareddigari VG, Le NT, Hart L, Bendell JC, Eckhardt G, Kurzrock R, Flaherty K, Burris HA 3rd, Messersmith WA: **Safety, pharmacokinetic, pharmacodynamic, and efficacy data for the oral MEK inhibitor trametinib: a phase 1 dose-escalation trial.** *Lancet Oncol* 2012, **13:**773–781.
13. Engelman JA, Chen L, Tan X, Crosby K, Guimaraes AR, Upadhyay R, Maira M, McNamara K, Perera SA, Song Y, Chirieac LR, Kaur R, Lightbown A, Simendinger J, Li T, Padera RF, Garcia-Echeverria C, Weissleder R, Mahmood U, Cantley LC, Wong KK: **Effective use of PI3K and MEK inhibitors to treat mutant Kras G12D and PIK3CA H1047R murine lung cancers.** *Nat Med* 2008, **14:**1351–1356.
14. Kinross KM, Brown DV, Kleinschmidt M, Jackson S, Christensen J, Cullinane C, Hicks RJ, Johnstone RW, McArthur GA: **In vivo activity of combined PI3K/mTOR and MEK inhibition in a Kras(G12D);Pten deletion mouse model of ovarian cancer.** *Mol Cancer Ther* 2011, **10:**1440–1449.
15. Chen Z, Cheng K, Walton Z, Wang Y, Ebi H, Shimamura T, Liu Y, Tupper T, Ouyang J, Li J, Gao P, Woo MS, Xu C, Yanagita M, Altabef A, Wang S, Lee C, Nakada Y, Pena CG, Sun Y, Franchetti Y, Yao C, Saur A, Cameron MD, Nishino M, Hayes DN, Wilkerson MD, Roberts PJ, Lee CB, Bardeesy N, Butaney M, Chirieac LR, Costa DB, Jackman D, Sharpless NE, Castrillon DH, Demetri GD, Janne PA, Pandolfi PP, Cantley LC, Kung AL, Engelman JA, Wong KK: **A murine lung cancer co-clinical trial identifies genetic modifiers of therapeutic response.** *Nature* 2012, **483:**613–617.
16. Tegnebratt T, Lu L, Lee L, Meresse V, Tessier J, Ishii N, Harada N, Pisa P, Stone-Elander S: **[18F] FDG-PET imaging is an early non-invasive pharmacodynamic biomarker for a first-in-class dual MEK/Raf inhibitor, RO5126766 (CH5126766), in preclinical xenograft models.** *EJNMMI Res* 2013, **3:**67.
17. Baudy AR, Dogan T, Flores-Mercado JE, Hoeflich KP, Su F, van Bruggen N, Williams SP: **FDG-PET is a good biomarker of both early response and acquired resistance in BRAFV600 mutant melanomas treated with vemurafenib and the MEK inhibitor GDC-0973.** *EJNMMI Res* 2012, **2:**22.
18. Speer R, Wulfkuhle J, Espina V, Aurajo R, Edmiston KH, Liotta LA, Petricoin EF 3rd: **Development of reverse phase protein microarrays for clinical applications and patient-tailored therapy.** *Cancer Genomics Proteomics* 2007, **4:**157–164.
19. Paweletz CP, Charboneau L, Bichsel VE, Simone NL, Chen T, Gillespie JW, Emmert-Buck MR, Roth MJ, Petricoin IE, Liotta LA: **Reverse phase protein microarrays which capture disease progression show activation of pro-survival pathways at the cancer invasion front.** *Oncogene* 2001, **20:**1981–1989.
20. Gopal YN, Deng W, Woodman SE, Komurov K, Ram P, Smith PD, Davies MA: **Basal and treatment-induced activation of AKT mediates resistance to cell death by AZD6244 (ARRY-142886) in Braf-mutant human cutaneous melanoma cells.** *Cancer Res* 2010, **70:**8736–8747.
21. Mirzoeva OK, Das D, Heiser LM, Bhattacharya S, Siwak D, Gendelman R, Bayani N, Wang NJ, Neve RM, Guan Y, Hu Z, Knight Z, Feiler HS, Gascard P, Parvin B, Spellman PT, Shokat KM, Wyrobek AJ, Bissell MJ, McCormick F, Kuo WL, Mills GB, Gray JW, Korn WM: **Basal subtype and MAPK/ERK kinase (MEK)-phosphoinositide 3-kinase feedback signaling determine susceptibility of breast cancer cells to MEK inhibition.** *Cancer Res* 2009, **69:**565–572.
22. Network CGA: **Comprehensive molecular portraits of human breast tumours.** *Nature* 2012, **490:**61–70.
23. Gujral TS, Karp RL, Finski A, Chan M, Schwartz PE, Macbeath G, Sorger P: **Profiling phospho-signaling networks in breast cancer using reverse-phase protein arrays.** *Oncogene* 2013, **32:**3470–3476.
24. Tibes R, Qiu Y, Lu Y, Hennessy B, Andreeff M, Mills GB, Kornblau SM: **Reverse phase protein array: validation of a novel proteomic technology and utility for analysis of primary leukemia specimens and hematopoietic stem cells.** *Mol Cancer Ther* 2006, **5:**2512–2521.
25. Isshiki Y, Kohchi Y, Iikura H, Matsubara Y, Asoh K, Murata T, Kohchi M, Mizuguchi E, Tsujii S, Hattori K, Miura T, Yoshimura Y, Aida S, Miwa M, Saitoh R, Murao N, Okabe H, Belunis C, Janson C, Lukacs C, Schuck V, Shimma N: **Design and synthesis of novel allosteric MEK inhibitor CH4987655 as an orally available anticancer agent.** *Bioorg Med Chem Lett* 2011, **21:**1795–1801.
26. Higashi K, Ueda Y, Sakurai A, Wang XM, Xu L, Murakami M, Seki H, Oguchi M, Taki S, Nambu Y, Tonami H, Katsuda S, Yamamoto I: **Correlation of Glut-1 glucose transporter expression with.** *Eur J Nucl Med* 2000, **27:**1778–1785.
27. Mulder J, Bjorling E, Jonasson K, Wernerus H, Hober S, Hokfelt T, Uhlen M: **Tissue profiling of the mammalian central nervous system using human antibody-based proteomics.** *Mol Cell Proteomics* 2009, **8:**1612–1622.
28. Ishii N, Harada N, Joseph EW, Ohara K, Miura T, Sakamoto H, Matsuda Y, Tomii Y, Tachibana-Kondo Y, Iikura H, Aoki T, Shimma N, Arisawa M, Sowa Y, Poulikakos PI, Rosen N, Aoki Y, Sakai T: **Enhanced inhibition of ERK signaling by a novel allosteric MEK inhibitor, CH5126766, that suppresses feedback reactivation of RAF activity.** *Cancer Res* 2013, **73:**4050–4060.
29. Kraeber-Bodere F, Carlier T, Naegelen VM, Shochat E, Lumbroso J, Trampal C, Nagarajah J, Chua S, Hugonnet F, Stokkel M, Gleeson F, Tessier J: **Differences in the biologic activity of 2 novel MEK inhibitors revealed by 18F-FDG PET: analysis of imaging data from 2 phase I trials.** *J Nucl Med* 2012, **53:**1836–1846.
30. de Geus-Oei LF, van Krieken JH, Aliredjo RP, Krabbe PF, Frielink C, Verhagen AF, Boerman OC, Oyen WJ: **Biological correlates of FDG uptake in non-small cell lung cancer.** *Lung Cancer* 2007, **55:**79–87.
31. Mamede M, Higashi T, Kitaichi M, Ishizu K, Ishimori T, Nakamoto Y, Yanagihara K, Li M, Tanaka F, Wada H, Manabe T, Saga T: **[18F] FDG uptake and PCNA, Glut-1, and Hexokinase-II expressions in cancers and inflammatory lesions of the lung.** *Neoplasia* 2005, **7:**369–379.
32. Ong LC, Jin Y, Song IC, Yu S, Zhang K, Chow PK: **2-[18F]-2-deoxy-D-glucose (FDG) uptake in human tumor cells is related to the expression of GLUT-1 and hexokinase II.** *Acta Radiol* 2008, **49:**1145–1153.
33. Tateishi U, Nishihara H, Tsukamoto E, Morikawa T, Tamaki N, Miyasaka K: **Lung tumors evaluated with FDG-PET and dynamic CT: the relationship between vascular density and glucose metabolism.** *J Comput Assist Tomogr* 2002, **26:**185–190.
34. Higashi K, Ueda Y, Yagishita M, Arisaka Y, Sakurai A, Oguchi M, Seki H, Nambu Y, Tonami H, Yamamoto I: **FDG PET measurement of the proliferative potential of non-small cell lung cancer.** *J Nucl Med* 2000, **41:**85–92.
35. Avril N: **GLUT1 expression in tissue and (18)F-FDG uptake.** *J Nucl Med* 2004, **45:**930–932.

36. Davies BR, Logie A, McKay JS, Martin P, Steele S, Jenkins R, Cockerill M, Cartlidge S, Smith PD: **AZD6244 (ARRY-142886), a potent inhibitor of mitogen-activated protein kinase/extracellular signal-regulated kinase kinase 1/2 kinases: mechanism of action in vivo, pharmacokinetic/pharmacodynamic relationship, and potential for combination in preclinical models.** *Mol Cancer Ther* 2007, **6:**2209–2219.
37. Solit DB, Garraway LA, Pratilas CA, Sawai A, Getz G, Basso A, Ye Q, Lobo JM, She Y, Osman I, Golub TR, Sebolt-Leopold J, Sellers WR, Rosen N: **BRAF mutation predicts sensitivity to MEK inhibition.** *Nature* 2006, **439:**358–362.
38. Akinleye A, Furqan M, Mukhi N, Ravella P, Liu D: **MEK and the inhibitors: from bench to bedside.** *J Hematol Oncol* 2013, **6:**27.
39. Friday BB, Yu C, Dy GK, Smith PD, Wang L, Thibodeau SN, Adjei AA: **BRAF V600E disrupts AZD6244-induced abrogation of negative feedback pathways between extracellular signal-regulated kinase and Raf proteins.** *Cancer Res* 2008, **68:**6145–6153.
40. Rexer BN, Ghosh R, Arteaga CL: **Inhibition of PI3K and MEK: it is all about combinations and biomarkers.** *Clin Cancer Res* 2009, **15:**4518–4520.
41. Smalley KS, Lioni M, Dalla Palma M, Xiao M, Desai B, Egyhazi S, Hansson J, Wu H, King AJ, Van Belle P, Elder DE, Flaherty KT, Herlyn M, Nathanson KL: **Increased cyclin D1 expression can mediate BRAF inhibitor resistance in BRAF V600E-mutated melanomas.** *Mol Cancer Ther* 2008, **7:**2876–2883.
42. Turke AB, Song Y, Costa C, Cook R, Arteaga CL, Asara JM, Engelman JA: **MEK inhibition leads to PI3K/AKT activation by relieving a negative feedback on ERBB receptors.** *Cancer Res* 2012, **72:**3228–3237.
43. Gioeli D, Wunderlich W, Sebolt-Leopold J, Bekiranov S, Wulfkuhle JD, Petricoin EF 3rd, Conaway M, Weber MJ: **Compensatory pathways induced by MEK inhibition are effective drug targets for combination therapy against castration-resistant prostate cancer.** *Mol Cancer Ther* 2011, **10:**1581–1590.
44. Flores LG 2nd, Yeh HH, Soghomonyan S, Young D, Bankson J, Hu Q, Alauddin M, Huff V, Gelovani JG: **Monitoring therapy with MEK inhibitor U0126 in a novel Wilms tumor model in Wt1 knockout Igf2 transgenic mice using (18)F-FDG PET with dual-contrast enhanced CT and MRI: early metabolic response without inhibition of tumor growth.** *Mol Imaging Biol* 2012, **15:**175–185.
45. Saini KS, Loi S, de Azambuja E, Metzger-Filho O, Saini ML, Ignatiadis M, Dancey JE, Piccart-Gebhart MJ: **Targeting the PI3K/AKT/mTOR and Raf/MEK/ERK pathways in the treatment of breast cancer.** *Cancer Treat Rev* 2013, **39:**935–946.
46. Renshaw J, Taylor KR, Bishop R, Valenti M, De Haven Brandon A, Gowan S, Eccles SA, Ruddle RR, Johnson LD, Raynaud FI, Selfe JL, Thway K, Pietsch T, Pearson AD, Shipley J: **Dual blockade of the PI3K/AKT/mTOR (AZD8055) and RAS/MEK/ERK (AZD6244) pathways synergistically inhibits rhabdomyosarcoma cell growth in vitro and in vivo.** *Clin Cancer Res* 2013, **19:**5940–5951.
47. Jahangiri A, Weiss WA: **It takes two to tango: dual inhibition of PI3K and MAPK in rhabdomyosarcoma.** *Clin Cancer Res* 2013, **19:**5811–5813.
48. Meng J, Dai B, Fang B, Bekele BN, Bornmann WG, Sun D, Peng Z, Herbst RS, Papadimitrakopoulou V, Minna JD, Peyton M, Roth JA: **Combination treatment with MEK and AKT inhibitors is more effective than each drug alone in human non-small cell lung cancer in vitro and in vivo.** *PLoS One* 2010, **5:**e14124.

doi:10.1186/s13550-014-0034-6
Cite this article as: Tegnebratt *et al.*: Evaluation of efficacy of a new MEK inhibitor, RO4987655, in human tumor xenografts by [^{18}F] FDG-PET imaging combined with proteomic approaches. *EJNMMI Research* 2014 **4**:34.